Short note: the pulse stretch phenomenon in the context of data-driven imaging methods

Jürgen Mann and German Höcht

email: *Juergen.Mann@gpi.uka.de*
keywords: *CRS stack, pulse stretch, NMO correction, wavefield attributes*

ABSTRACT

Moveout corrections based on hyperbolic traveltime approximations are usually expected to cause distortions of the wavelet, especially for comparatively small traveltimes and large offsets. This kind of pulse stretch effect is well known from the conventional NMO correction and requires appropriate muting of the pre-stack data. However, data-driven imaging methods based on multi-parameter traveltime approximations like Multifocusing, delayed hyperbola approaches, or Common-Reflection-Surface stack do not expose such a stretch phenomenon. In this contribution, we briefly review the origin of the pulse stretch effect and relate it to the artifical smoothness of typically applied NMO velocity fields. Data-driven imaging methods introduce a systematic variation of the stacking velocity to avoid the unwanted pulse stretch. In contrast, the associated kinematic CRS wavefield attributes remain virtually constant and, thus, again turn out to provide a more appropriate parameterization of the recorded wavefield.

INTRODUCTION

Conventional imaging methods often systematically distort the wavelet with respect to its length and its shape. The former leads to a reduced frequency content in the resulting image and the latter bears the risk of a misinterpretation. These inherent effects occur even if the stacking operators are kinematically correct: they are due to the usually smooth parameterization of the model, irrespective if this model is explicitly given (model-based imaging methods like Kirchhoff migration) or implicitly derived from the pre-stack data (data-driven methods like NMO/DMO/stack).

This kind of unwanted changes of the wavelet do not occur during the CRS stack and similar data-oriented imaging methods like Multifocusing (Berkovitch et al., 1994; Landa et al., 1999) or the delayed hyperbola approaches by de Bazelaire (1988); Thore et al. (1994). To explain this fact, we will briefly review the reasons for the pulse stretch in conventional imaging methods for a simple example where the respective second-order operators are kinematically exact. We discuss different approximations for the stacking trajectories for neighboring samples along the wavelet in band-limited data and compare them to the stacking velocities determined by means of the Common-Reflection-Surface stack. It turns out that the optimum stacking velocity model for an undistorted stacked wavelet is not smooth but contains a systematic variation of the stacking velocity.

Reformulated in terms of kinematic wavefield attributes, namely emergence angles and radii of wavefront curvatures, these variations can be removed to a large extend and allow a more reliable extraction of information for subsequent processing steps, e. g., for the tomographic inversion approach presented by Duveneck in this issue. Furthermore, the kinematic wavefield attributes provide a description that always has a sound physical meaning, even in cases where the stacking velocity is imaginary or tends to infinity, i. e., in situations with negative or vanishing moveout.

CMP TRAVELTIMES ALONG THE WAVELET

As already indicated above, pulse stretch even occurs for events with perfectly hyperbolic traveltime curves. To focus on this effect, we will only consider such idealized situations in the following. The simplest situation that leads to perfectly hyperbolic events is, of course, a plane reflector with homogeneous overburden. Without imposing any restrictions on the considerations, we can assume a horizontal reflector for the sake of simplicity, as the dip only occurs as additional factor in the stacking velocity. For a reflector at depth z_0 and a velocity v_0, the kinematic reflection response is simply given by

$$t(h) = \frac{2}{v_0}\sqrt{h^2 + z_0^2} = \sqrt{t_0^2 + \frac{4\,h^2}{v_0^2}}\,, \tag{1}$$

where $t_0 = 2\,z_0/v_0$ denotes the ZO traveltime and h is the half-offset.

For a medium without attenuation, the pre-stack data can be represented as a temporal convolution of the source wavelet with the temporal length T and the kinematic reflection response.[1] In other words, the pulse length is identical for all shot and receiver locations. An undistorted imaging result can be obtained by stacking along the kinematic reflection response (1) vertically shifted to all locations in the time domain within the temporal length of the wavelet:

$$t(h, \Delta t) = \sqrt{t_0^2 + \frac{4\,h^2}{v_0^2}} + \Delta t \quad \text{with} \quad -\frac{T}{2} \le \Delta t \le \frac{T}{2}\,, \tag{2}$$

where we assume that the wavelet is centered around the traveltime t, i. e. a zero-phase wavelet. Of course, the same considerations can also be made for causal wavelets.

An NMO correction applied with the correct velocity v_0 obviously yields the correct traveltimes (1) and, thus, the correct operator for the center of the wavelet. However, the NMO operators attached to all other ZO traveltimes differ from the iso-phase curves (2) in the data: the moveout difference between the two operators attached to the ZO traveltimes $t_0^{(\pm)} = t_0 \pm T/2$

$$\Delta t_{\text{NMO}} = \sqrt{t_0^{(+)2} + \frac{4\,h^2}{v_0^2}} - \sqrt{t_0^{(-)2} + \frac{4\,h^2}{v_0^2}} \le T \tag{3}$$

is not constant, but decreases with increasing offset. This leads to the well known NMO pulse stretch. Similar considerations also apply to other imaging methods based on hyperbolic operators (see, e. g., Mann, 2002). The pulse stretch is due to the fact that the shape of the operators not only depends on the velocity v_0, but also on the ZO traveltime. This is an inherent property of the hyperbolic traveltime expressions used for NMO, CMP stack, and other imaging methods. Parabolic representations avoid the pulse stretch as their shape remains unchanged for neighboring points. However, such representations are kinematically less accurate, especially in the considered case where the hyperbolic representations are exact.

ALTERNATIVE APPROXIMATIONS OF THE STACKING VELOCITY

The application of a constant stacking velocity model is obviously not suited to describe the iso-phase curves in the input data, not even in the simplest possible situation. Thus, we have to look for a better description of the stacking velocity along the seismic wavelet. To address this task, we try to express the shifted hyperbola (2) in the same form as the hyperbolic operator (1) and in terms of the ZO traveltime t_0 and the velocity v_0 defined at the center of the wavelet. Solving for the new stacking velocity v_{shift}, we obtain

$$v_{\text{shift}}^2\,(\Delta t, h) = \frac{2\,h^2\,v_0^2}{2h^2 + v_0^2\,\Delta t\sqrt{t_0^2 + \frac{4h^2}{v_0^2}} - v_0^2\,t_0\,\Delta t}\,. \tag{4}$$

This velocity explicitely depends on the half-offset h, in other words, the shifted hyperbola (2) cannot be expressed by means of a single stacking velocity. If we fix h, the time shift Δt is the same for this offset

[1] For critical and super-critical reflection angles, an additional phase shift occurs. We will not consider this case here. For the model presented later on, such situations do not occur at all.

and offset zero, but not for arbitrary offsets. For an exact description of the iso-phase curves in the data, we would have to allow an additional parameter, the time shift Δt itself. To avoid this additional parameter, a reasonable approximation of v_{shift} is required.

In conventional processing, v_{shift} is assumed to coincide with v_0. Obviously, this is only true for $h \to \infty$, simply stating that the asymptotes of the considered hyperbolae are parallel and, thus, have a constant time shift. For the simulation of ZO sections, this constitutes an inappropriate approximation that leads to pulse stretch. As in NMO stacking velocity models velocity usually increases with increasing time, the actual situation is even worse.

For a ZO simulation, a more reasonable approach is to require a constant curvature at offset zero of all stacking hyperbolae, i. e., all values of Δt. This ensures that the time shift is constant in a vicinity of offset zero. With this approximation, the stacking velocity reads

$$v^2_{\text{shift,c}} = \frac{t_0}{t_0 + \Delta t} v_0^2 \,, \tag{5}$$

where the index c indicates constant ZO curvature. The same result can be obtained by means of an expansion of the shifted hyperbola (2) if we keep only terms up to second order in h.

So far, we have two quite different approximations for the shifted hyperbolae: constant stacking velocity (the conventional approach) and constant curvature at offset zero. Below, we will compare these approaches to the stacking velocity found by means of coherence analysis in the pre-stack data.

NUMERICAL EXAMPLE FOR A 1-D MODEL

To analyze the behavior of the stacking velocity derived by means of the CRS stack method, we defined a simple 1-D model consisting of three horizontal planar reflectors at depths $z_i = 1000, 1080, 1160\,\text{m}$ with a constant velocity $v_0 = 1500\,\text{m/s}$. The impedance contrasts are entirely due to density changes, thus, neither refraction nor over-critical reflections occur at the interfaces, and all events are perfectly hyperbolic. The wavelet is a Ricker wavelet with a peak frequency of 30 Hz. A CMP gather within a half-offset range of $0 \ldots 500\,\text{m}$ was simulated with a fold of 31. We added some noise to the data to obtain reasonable coherence values and to avoid artifacts. As reference, the modeled ZO trace is shown on the left-hand side of Figure 1a. Note that for this model no significant pulse stretch will occur with conventional NMO correction: the maximum stretch is $\approx 10\%$, which is usually considered as acceptable. Our aim is to demonstrate that the optimum varying stacking velocity can even be recovered in case of very subtle variations.

This CMP gather served as input to the first step of the CRS stack processing scheme, the automatic CMP stack. This process also uses the one-parameter operator (1). However, it determines the optimum stacking velocity separately for each simulated ZO sample. Thus, no smoothness of the stacking velocity is imposed. The resulting stacked trace is shown on the right-hand side of Figure 1a: as expected, the wavelet is recovered without any stretch. The associated coherence values, namely semblance, calculated along the stacking trajectories is depicted in Figure 1b. It easily allows to identify the events and tells us for which traveltimes the stacking velocity is meaningful. The detected stacking velocity is shown as solid line in Figures 1c and d. As expected from the considerations in the previous section, it is not constant along the wavelet, but exposes a characteristic "jig saw" appearance: it *decreases* along the wavelet with *increasing* traveltime. This is in contrast to usually applied smooth NMO velocity models.

Let us now compare the detected velocity to the expected behavior for constant ZO curvature according to Equation 5. The analytic values are displayed as dashed lines in Figure 1c, of course separately for each event. We observe a very good fit to the semblance-based results extracted from the pre-stack data.

But now let us go a step further: the assumption of constant curvature only provides a constant time shift close to offset zero. However, a finite half-offset range of $0 \ldots 500\,\text{m}$ contributes to the stack. Thus, one might argue that Equation (4) might provide an even better fit for a certain "average offset" such that the deviation from the constant time shift is as small as possible for all offsets. We analyzed this by minimizing the least square error between the shifted hyperbolae and its one-parameter approximation. Strikingly, the optimum half-offset obtained in this way is a) virtually independent of the time shift Δt, b) the same for all three events, and c) with $\approx 830\,\text{m}$ located outside the modeled half-offset range. The stacking velocity calculated in this way is depicted as dashed line in Figure 1d. The result is very similar to the constant

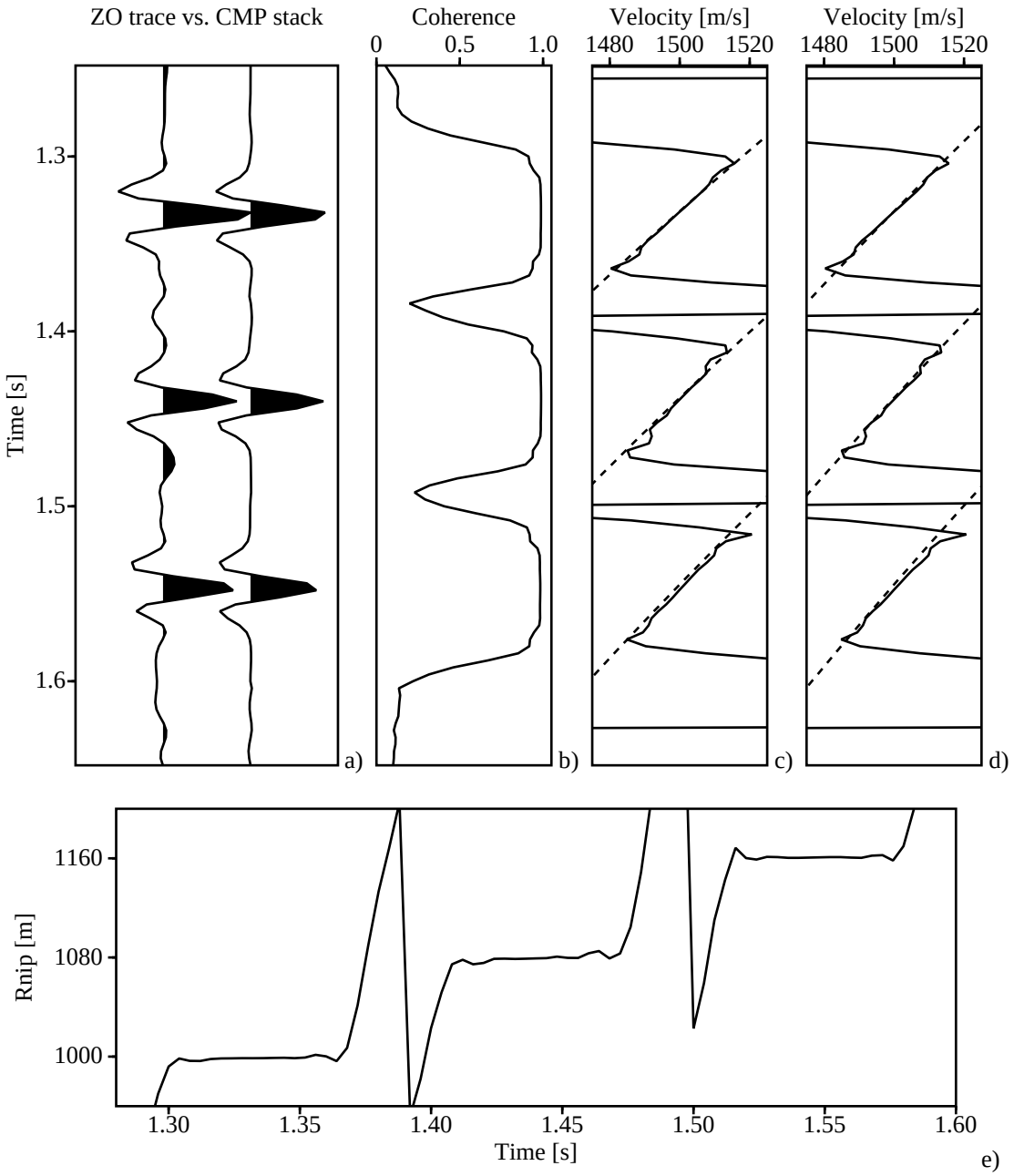

Figure 1: Synthetic example: a) slightly noisy modeled ZO trace vs. the CMP stack result, b) coherence measure semblance calculated along the stacking hyperbolae, c) detected stacking velocities (solid line) vs. forward-calculated stacking velocities (dashed lines) for hyperbolae with the same curvature at offset zero, and d) same as c) but for hyperbolae providing the best kinematic fit within the given offset range. e) radius of the NIP wavefront. In contrast to the stacking velocity, R_{NIP} is almost constant along the wavelet and—for this simple model—represents the reflector depths.

curvature approach shown in Figure 1d and fits the detected velocities even a little better.

BEHAVIOR OF THE KINEMATIC WAVEFIELD ATTRIBUTES

In the following, we will reformulate the preceeding sections in terms of the CRS wavefield attributes. The CRS operator is also a hyperbolic representation and its shape also explicitly depends on the ZO traveltime t_0. Expressed in terms of midpoint coordinate x_m and half-offset h, it reads

$$t^2_{\mathrm{hyp}}\left(x_\mathrm{m}, h\right) = \left[t_0 + \frac{2\,\sin\alpha\,\left(x_\mathrm{m} - x_0\right)}{v_0}\right]^2 + \frac{2\,t_0\,\cos^2\alpha}{v_0}\left[\frac{\left(x_\mathrm{m} - x_0\right)^2}{R_\mathrm{N}} + \frac{h^2}{R_\mathrm{NIP}}\right], \tag{6}$$

where v_0 represents the near-surface velocity and (t_0, x_0) is the considered ZO location. The CRS operator is parameterized by three kinematic wavefield attributes defined at the surface location x_0, namely α, the emergence angle of the normal ray, R_NIP, the radius of the normal-incidence-point (NIP) wavefront, and R_N, the radius of the normal wavefront. The relation of these attributes to two so-called eigenwave experiments can, e. g., be found in Mann et al. (1999) and Jäger et al. (2001).

For the considered 1-D model, it is obvious that all rays are vertical and all normal wavefronts are plane, i. e., $\alpha = 0$ and $R_\mathrm{N} = \pm\infty$ for all three events. Accordingly, the CRS operator reduces to

$$t\left(x_\mathrm{m}, h\right) = \sqrt{t_0^2 + \frac{2\,t_0\,h^2}{v_0\,R_\mathrm{NIP}}} \tag{7}$$

for any midpoint location x_m. For the center of the wavelet, this represents the exact kinematic reflection response of the reflector with $R_\mathrm{NIP} = z = v_0\,t_0/2$. As a matter of fact, this is simply an alternative formulation of the well known CMP moveout formula (1).

More general, the stacking velocity v_stack is related to the wavefield attributes according to

$$v^2_\mathrm{stack} = \frac{R_\mathrm{NIP}\,v_0}{2\,t_0\,\cos\alpha}\,. \tag{8}$$

If we reformulate Equation (5) in terms of R_NIP for t_0 and $R_\mathrm{NIP,shift}$ for $t_0 + \Delta t$, we readily observe that $R_\mathrm{NIP} = R_\mathrm{NIP,shift}$ for any Δt: the angle α is determined by the linear term in the CRS operator (6), such that it does not vary along the wavelet. In other words, the assumption of constant curvature of the traveltime curves at offset zero is equivalent to constant radius of curvature R_NIP along the wavelet. As this approximation provided a good fit to the detected stacking velocity, we can also expect the corresponding behavior for R_NIP. Indeed, the NIP wavefront radius shown in Figure 1e, calculated from the detected stacking velocities according to Equation (8), is almost constant for each of the three events, for this 1-D model simply representing the reflector depths z_i. Thus, this radius appears to be a more natural parameter for the traveltime curves as it does not vary along the wavelet. Furthermore, it is always well-defined even in situations when the stacking velocity has no physical meaning.

So far, we only considered the CMP gather. As the CRS operator is hyperbolic for any configuration that includes the simulated ZO location, e. g., common-shot or common-receiver gather or the ZO section, the same behavior is expected in any case. The additional linear term in any gather except the CMP gather does not change the principal properties. The respective curvature, in general a linear combination of $1/R_\mathrm{NIP}$ and $1/R_\mathrm{N}$ will remain almost constant along the wavelet and the pulse stretch will be avoided. This allows a far more reliable extraction of attributes for subsequent applications than the stacking velocity section.

CONCLUSIONS

We briefly reviewed the origin of pulse stretch in conventional time domain processing with constant or smooth NMO velocity models. A stretch free imaging with optimally recovered wavelet is not possible with such models: the limited bandwidth of the data is not considered even in case of kinematically exact operators. We discussed an approximation of the stacking velocity variation along the wavelet that is better suited for the simulation of ZO sections. A comparison with CRS stack results for a 1-D model demonstrated that data-driven imaging methods automatically avoid the pulse stretch and introduce a systematic

variation of the stacking velocity. Formulated in terms of the kinematic CRS wavefield attributes, this variation vanishes. Thus, the radii of wavefront curvatures involved in the CRS stack approach provide a more natural parameterization of the reflection events.

ACKNOWLEDGEMENTS

This work was kindly supported by the sponsors of the *Wave Inversion Technology (WIT) Consortium*, Karlsruhe, Germany.

REFERENCES

Berkovitch, A., Gelchinsky, B., and Keydar, S. (1994). Basic formulae for multifocusing stack. In *Extended Abstracts*. 56th Mtg. Eur. Assoc. Expl. Geophys. Session: P140.

de Bazelaire, E. (1988). Normal moveout revisited – inhomogeneous media and curved interfaces. *Geophysics*, 53(2):143–157.

Jäger, R., Mann, J., Höcht, G., and Hubral, P. (2001). Common-reflection-surface stack: Image and attributes. *Geophysics*, 66(1):97–109.

Landa, E., Gurevich, B., Keydar, S., and Trachtman, P. (1999). Application of multifocusing method for subsurface imaging. *J. Appl. Geoph.*, 42(3,4):283–300.

Mann, J. (2002). *Extensions and applications of the Common-Reflection-Surface Stack method*. Logos Verlag, Berlin.

Mann, J., Jäger, R., Müller, T., Höcht, G., and Hubral, P. (1999). Common-reflection-surface stack – a real data example. *J. Appl. Geoph.*, 42(3,4):301–318.

Thore, P. D., de Bazelaire, E., and Ray, M. P. (1994). Three-parameter equation: An efficient tool to enhance the stack. *Geophysics*, 59(2):297–308.